

Electronic Supplementary Material (ESI) for ChemComm.
This journal is © The Royal Society of Chemistry 2018

Supplementary Information

Amorphous Y(OH)₃-promoted Ru/Y(OH)₃ nanohybrids with high durability for electrocatalytic hydrogen evolution in alkaline media

Ying Liu,[‡] Xuyun Lu,[‡] Zhiwen Che, Caihua Zhang, Min Han, Jianchun Bao,* Zhihui Dai*

Jiangsu Collaborative Innovation Center of Biomedical Functional Materials, School of Chemistry and Materials Science, Nanjing Normal University, Nanjing 210023, P. R. China.

E-mail: daizhihui@njnu.edu.cn and baojianchun@njnu.edu.cn

[‡]Ying Liu and Xuyun Lu contributed equally to this work.

Experimental Section

1. Chemicals

The 20% Pt/C powder and 5 wt% Nafion were purchased from Alfa Aesar. $\text{Y}(\text{NO}_3)_3 \cdot 6\text{H}_2\text{O}$, $\text{Pd}(\text{NO}_3)_2 \cdot 2\text{H}_2\text{O}$, NaBH_4 , polyvinylpyrrolidone (PVP), cetyltrimethylammonium bromide (CTAB), KOH, acetone and anhydrous ethanol were purchased from Sinopharm Chemical Reagent Co., Ltd. $\text{RuCl}_3 \cdot n\text{H}_2\text{O}$ ($\text{Ru} \approx 37.0\% \pm 0.2\%$) was purchased from Shanghai Jiuyue Chemical Industry Co., Ltd. The ultrapure water used in this work was obtained from a Millipore water purification system ($\geq 18.25 \text{ M}\Omega \text{ cm}$, Millipore SAS Corporation, France). Unless otherwise stated, all the above chemicals were used as received without further purification.

2. Synthetic methods

Synthesis of the $\text{Ru}/\text{Y}(\text{OH})_3$ hybrid nanostructure. The $\text{Ru}/\text{Y}(\text{OH})_3$ hybrid nanostructure was prepared via an in situ NaBH_4 reduction method. In detail, $\text{Y}(\text{NO}_3)_3 \cdot 6\text{H}_2\text{O}$ (0.06 g, 0.16 mmol), PVP (0.22 g), CTAB (0.36 g) and $\text{RuCl}_3 \cdot n\text{H}_2\text{O}$ (0.33 g, 1.60 mmol) were first dissolved in deionized water (10 mL) and ultrasonicated to create a homogenous brown solution. After this solution was heated to 110°C in an oil bath, 10 mL of aqueous NaBH_4 (containing 0.2 g NaBH_4) was dropwise added to this solution under continuous magnetic stirring. During this process, abundant hydrogen bubbles were formed and released; thus, a certain amount of ethanol is necessary to reduce the surface tension of the solution. The above solution was maintained at 110°C for 2 h. Finally, a black precipitate was observed, which was centrifuged and separated several times using the mixture ethanol and acetone. The as-obtained product was dried at 60°C in a vacuum oven overnight.

Synthesis of sole Ru NPs. The synthesis procedure for the Ru NPs was similar to that for the $\text{Ru}/\text{Y}(\text{OH})_3$ nanostructure, but $\text{Y}(\text{NO}_3)_3 \cdot 6\text{H}_2\text{O}$ was not added.

Synthesis of the sole, flocculent $\text{Y}(\text{OH})_3$ scaffold. The synthesis procedure for the $\text{Y}(\text{OH})_3$ scaffold was similar to that for the $\text{Ru}/\text{Y}(\text{OH})_3$ nanostructure, but $\text{RuCl}_3 \cdot n\text{H}_2\text{O}$ was not added.

Synthesis of Ru/RGO . The synthesis procedure for the Ru/RGO was similar to that for the $\text{Ru}/\text{Y}(\text{OH})_3$ nanostructure, but $\text{Y}(\text{NO}_3)_3 \cdot 6\text{H}_2\text{O}$ was replaced with RGO (10 mg).

3. Characterization

Transmission electron microscopy (TEM) was performed using a JEM-200CX microscope (Japan) with an accelerating voltage of 200 kV. The powder X-ray diffraction (XRD) patterns were collected on a D/max 2500VL/PC diffractometer (Japan) equipped with graphite-monochromatized $\text{Cu K}\alpha$ radiation ($\lambda = 1.54060 \text{ \AA}$), and corresponding scan range (2θ) was 5° to 90° . The related high resolution

transmission electron microscopy (HRTEM), X-ray energy-dispersive spectra (EDS), elemental mapping, scanning transmission electron microscopy (STEM) and EDS line-scan images were acquired using a JEOL-2100F apparatus at an accelerating voltage of 200 kV. The thermogravimetric data were collected on TGA NETZSCH STA449F3 instruments. Fourier transform infrared (FTIR) spectra were recorded on Tensor 27 (Bruker, Germany) at room temperature. Raman spectra were recorded on a JY HR 800 (France) instrument with an optical multichannel spectrometer Microdil 28 (Dilor) equipped with a microscope. X-ray photoelectron spectroscopy (XPS) was conducted using a scanning X-ray microprobe (PHI 5000 Versa, ULAC-PHI, Inc.) with Al K α radiation. All energies were calibrated using the C1S peak (binding energy (BE) = 284.6 eV) as standard. Inductively coupled plasma (ICP) measurement was collected on an Induction Coupled Plasma Quantometer (Jarrell-Ash 1100 + 2000). The electrochemical impedance spectra (EIS) test was performed on a PGSTAT30/FRA2 system (Autolab, Netherlands) in 0.1 M KOH.

4. Electrochemical tests

The electrochemical HER experiments were conducted using a CHI 660D electrochemical workstation with a typical three-electrode cell setup. Pt foil was used as the counter electrode, Ag/AgCl (3 M KCl) acted as the reference electrode, and a glassy carbon electrode (GCE) (3 mm in diameter) served as the working electrode in 0.1 M KOH. To prepare the catalyst ink, a certain amount of catalyst was mixed with ethanol and ultrapure water (volume ratio of 1:3) and then ultrasonicated for approximately 20 min to obtain a homogeneous catalyst ink (2 mg mL⁻¹). Then, 10 μ L of the above catalyst ink was pipetted onto the GCE surface and air dried, followed by 5 μ L of a 1.0 wt% Nafion solution to protect the catalyst. All electrochemical measurements were conducted in a N₂-saturated atmosphere at room temperature. Prior to each electrochemical test, the modified electrodes were pretreated by performing several CV cycles until the potential was stable to remove any possible surface contamination. The CV tests were conducted using a potential window from -1.3 V to -0.5 V (vs. Ag/AgCl), and polarization curves were obtained using a potential window from -0.5 V to -1.3 V (vs. Ag/AgCl) after iR compensation with a scan rate of 5 mV s⁻¹. All potentials were referenced to reversible hydrogen electrode (RHE) values using the equation $E(\text{RHE}) = E_{\text{Ag/AgCl}} + 0.197 + 0.059\text{pH}$.

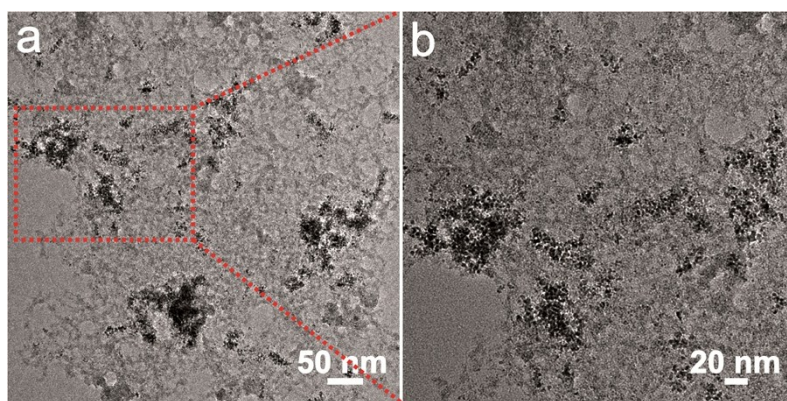


Fig. S1 TEM images of the product when all of the NaBH_4 solution (10 mL) was added at one time.

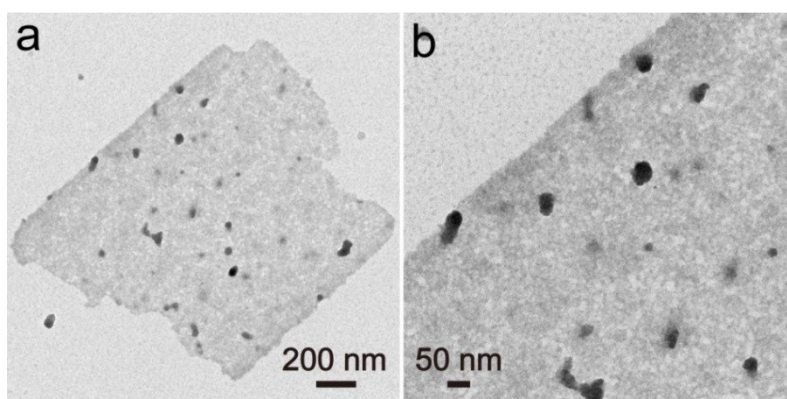


Fig. S2 TEM images of the product when NaBH_4 is replaced with $\text{N}_2\text{H}_4 \cdot \text{H}_2\text{O}$ and other experimental conditions are kept constant.

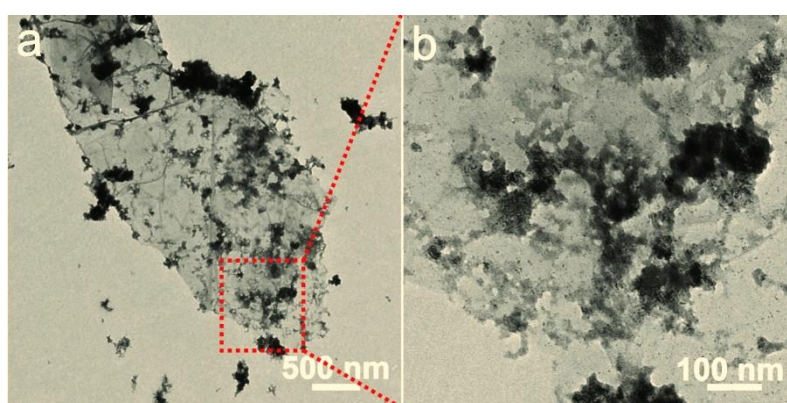


Fig. S3 TEM images of the product when $\text{Y}(\text{OH})_3$ is replaced with RGO and other experimental conditions are kept constant.

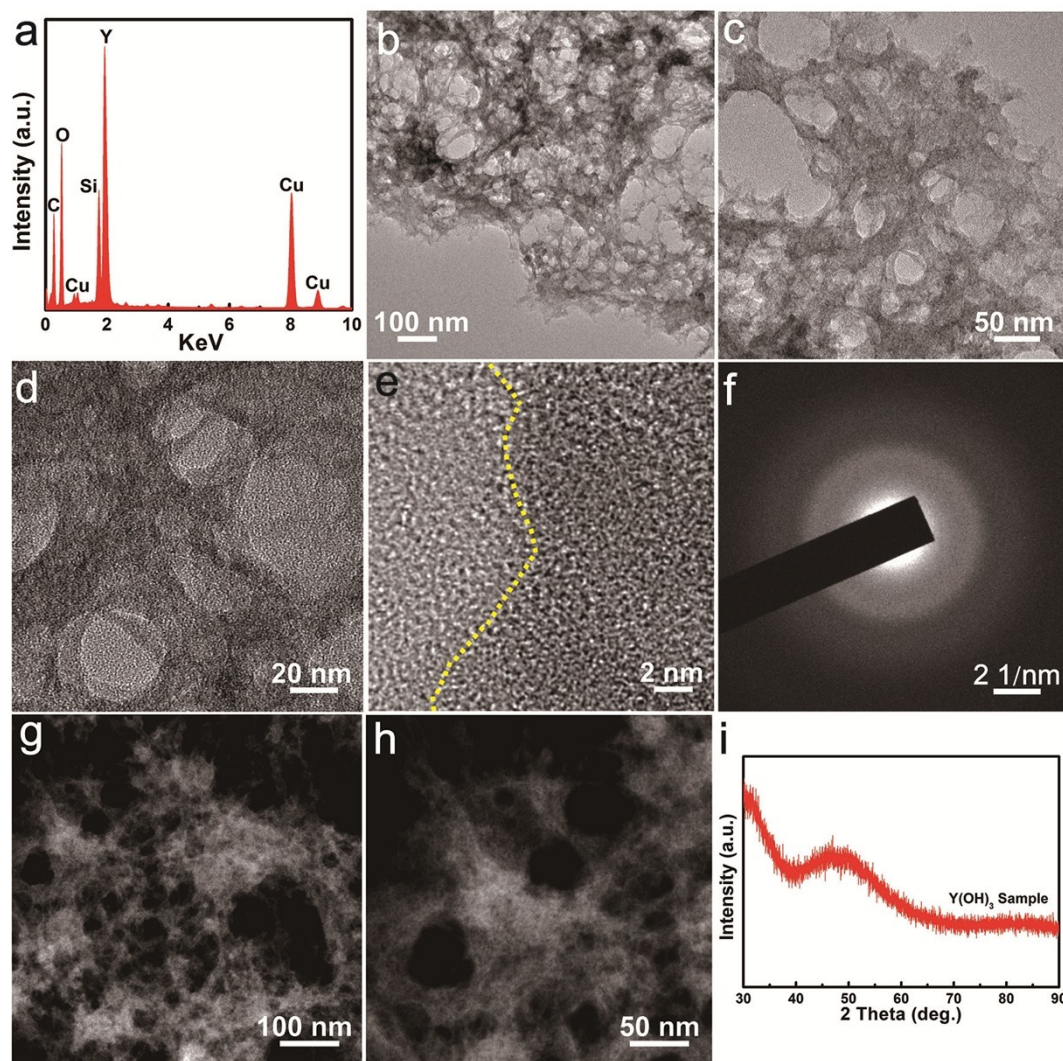


Fig. S4 (a) EDS, (b-d) TEM, (e) HRTEM, (f) SAED, (g, h) STEM and (i) XRD images of sole $\text{Y}(\text{OH})_3$ product.

Fig. S4 displays the component, morphology and crystal structure characterization of the as-prepared sole $\text{Y}(\text{OH})_3$ counterpart. The EDS spectrum in **Fig. S4a** reveals the existence of Y and O elements in the product while C, Cu and Si elements originate from copper grid substrate. **Fig. S4b-d** show the TEM images of the product, from which large area flocculent product is observed. **Fig. S4g and h** show the STEM images of the flocculent product, which also indicate its 3D morphology. The HRTEM and SAED images reveal that no obvious lattice fringes (**Fig. S4e**) and diffraction spot or diffraction ring (**Fig. S4f**) can be found, indicative of amorphous feature of this product. Related XRD pattern also verified this result (**Fig. S4i**). Thus to identify the composition and structure characteristics of this product, thermo-gravimetric (TG) and fourier transform infrared (FT-IR) analyses are employed, and details are described in **Fig. S5**.

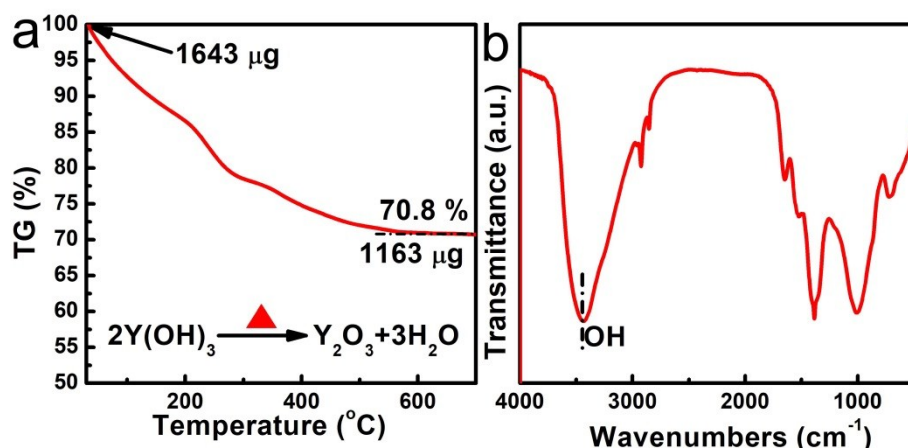


Fig. S5 (a) The thermogravimetric analysis under Ar gas atmosphere from room temperature to 800 °C and (b) FT-IR spectrum for the sole $Y(OH)_3$ product.

The TG curve in **Fig. S5a** demonstrates an attenuation of about 29.2% in mass during the decomposition process and finally remained at around 70.8%. Its decreased mass (480 μg) is exactly approximate to that of H_2O lost for $Y(OH)_3$, meaning a $Y(OH)_3$ structure for this product. The characteristic O-H stretching vibration at about 3540 cm^{-1} in related FT-IR spectrum also confirmed its $Y(OH)_3$ construction (**Fig. S5b**).

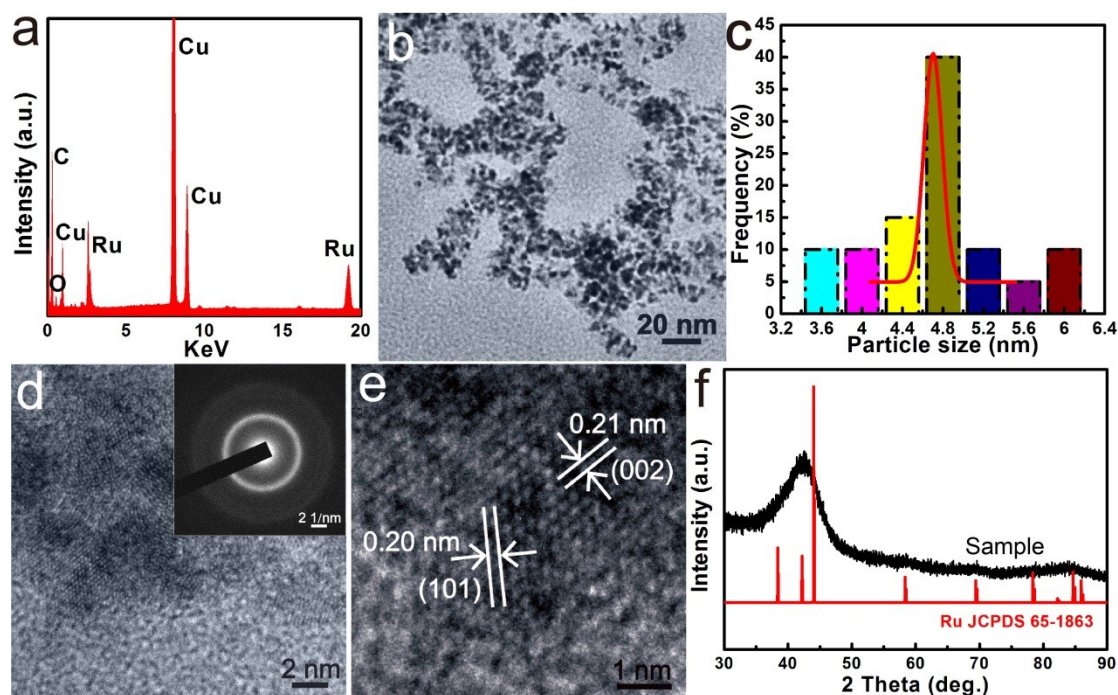


Fig. S6 (a) EDS, (b) TEM, (c) particle size distribution, (d, e) HRTEM, and (f) XRD images of sole Ru product.

Fig. S6 shows the component, morphology and crystal structure characterizations of the as-prepared sole Ru, from which large amounts of irregular Ru nanoparticles with an average size of about 4.8 nm and good crystallinity are observed.

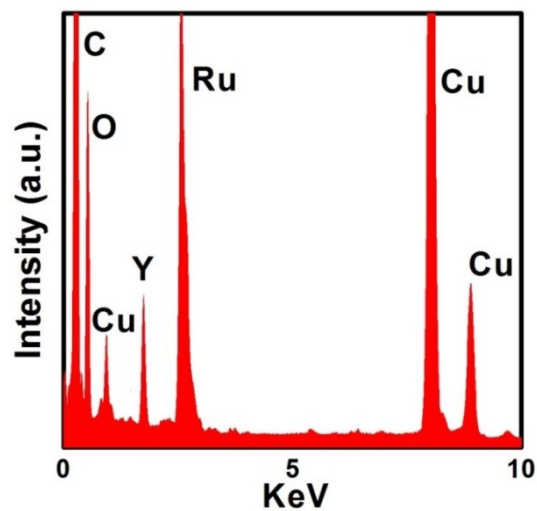


Fig. S7 EDS image of the Ru/Y(OH)₃ product.

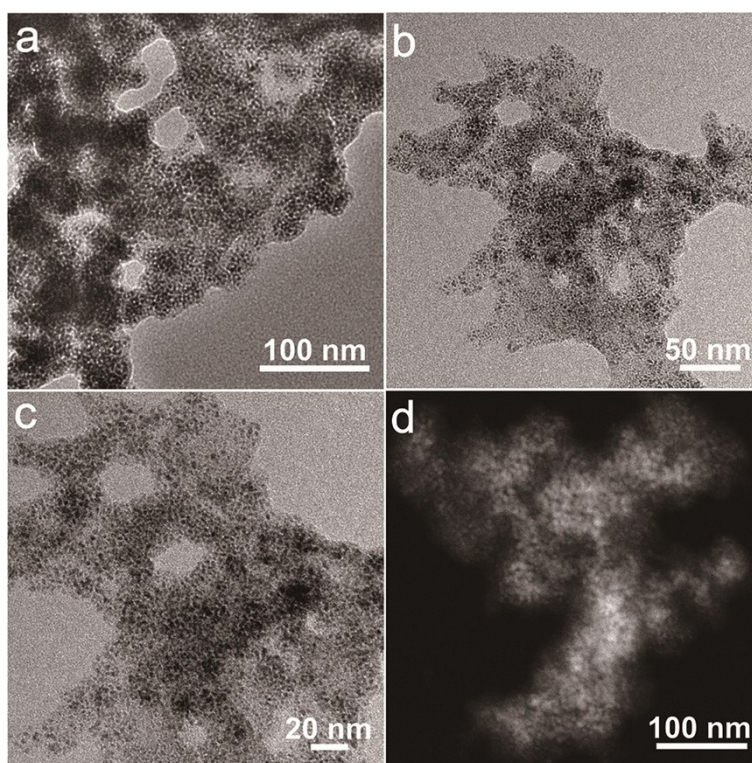


Fig. S8 (a-c) TEM and (d) STEM images of the Ru/Y(OH)₃ product.

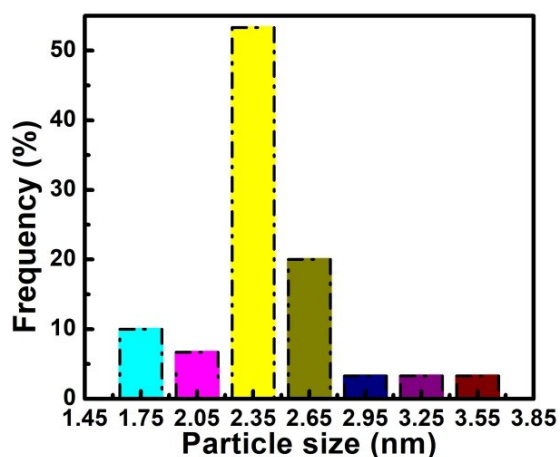


Fig. S9 Diameter distribution image of the Ru nanoparticles in Ru/Y(OH)₃ product.

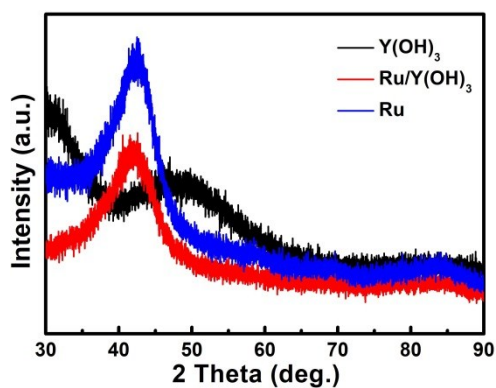


Fig. S10 The comparison of the XRD patterns of Ru/Y(OH)₃, Ru and Y(OH)₃.

In **Fig. S10**, the broad diffraction peak located at about 43° is assigned to the (101) or (002) planes of hexagonal Ru (JCPDS 65-1863) for Ru/Y(OH)₃ and sole Ru products, but nearly no obvious diffraction peak can be observed for the sole Y(OH)₃, indicative of the good crystallinity of Ru nanoparticles and amorphous feature of Y(OH)₃.

Table S1. The mass percentage of Ru and Y(OH)₃ in Ru/Y(OH)₃ product based on ICP test.

Sample	Ru (%)	Y(OH) ₃ (%)
Ru/Y(OH) ₃	85	15

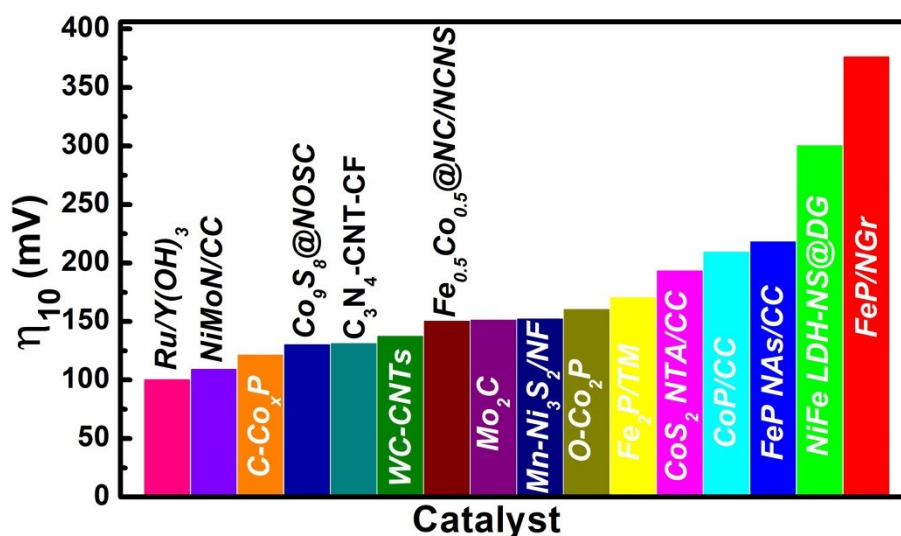


Fig. S11 Comparison of the overpotential at 10 mA cm⁻² (η_{10}) of the Ru/Y(OH)₃ NHs and some recently reported representative electrocatalysts for HER in alkaline media. The derivation of these electrocatalysts are listed in References 1 in turn.

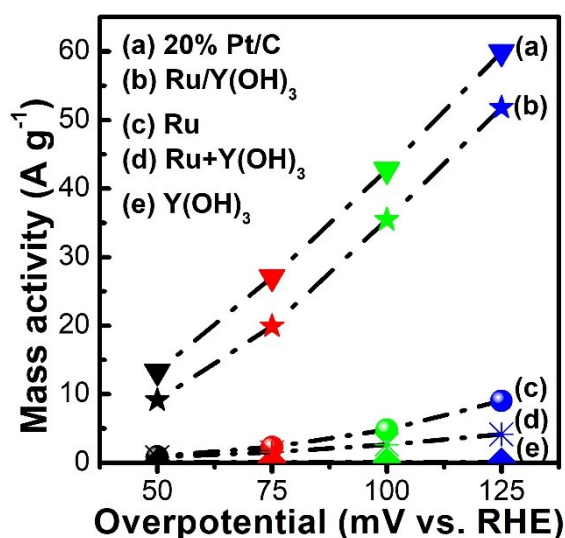


Fig. S12 Mass activity of the Ru/Y(OH)₃ NHs, Ru, Y(OH)₃, Ru+Y(OH)₃ and 20% Pt/C catalysts.

The mass activity value (A g⁻¹) in **Fig. S12** is calculated from the electrocatalyst loading m (0.28 mg cm⁻²) and the measured current density j (mA cm⁻²) at different overpotential (η) using the following formula:

$$\text{Mass activity} = j/m$$

Table S2. Comparison of the durability of some recently reported representative HER electrocatalysts in alkaline electrolytes

Catalyst	Durability	References
Mn-Ni ₃ S ₂ /NF	500	<i>Chem. Commun.</i> , DOI: 10.1039/c8cc06331a
Ni(OH) ₂ -Fe ₂ P/TM	500	<i>Chem. Commun.</i> , 2018 , 54, 1201.
Mn-doped Ni ₂ P	500	<i>Chem. Commun.</i> , 2017 , 53, 11048.
Ru/C ₃ N ₄ /C	1000	<i>J. Am. Chem. Soc.</i> , 2016 , 138, 16174.
(Fe _x Ni _{1-x}) ₂ P	1000	<i>Nano Energy</i> , 2017 , 38, 553.
MoS ₂ Confined Co(OH) ₂	1000	<i>ACS Nano</i> , 2018 , 12, 4565.
WC-CNTs	1000	<i>ACS Nano</i> , 2015 , 9, 5125.
Ru ND/C	1000	<i>Chem. Commun.</i> , 2018 , 54, 4613.
Ru ₂ P/rGO	2000	<i>Chem. Commun.</i> , 2018 , 54, 3343.
R-MoS ₂ /NF	5000	<i>Adv. Mater.</i> , 2018 , 30, 1707105.
CoP NWs/CC	5000	<i>Adv. Mater.</i> , 2018 , 30, 1703322.
C-Co _x P	10000	<i>Small</i> , 2018 , 14, 1801284.
4H/fcc Ru NTs	10000	<i>Small</i> , 2018 , 14, 1801090.
Ru@C ₂ N	10000	<i>Nat. Nanotechnol.</i> , 2017 , 12, 441.
Ru@CQDs	10000	<i>Adv. Mater.</i> , 2018 , 30, 1800676.
Ru/Y(OH) ₃	20000	this work

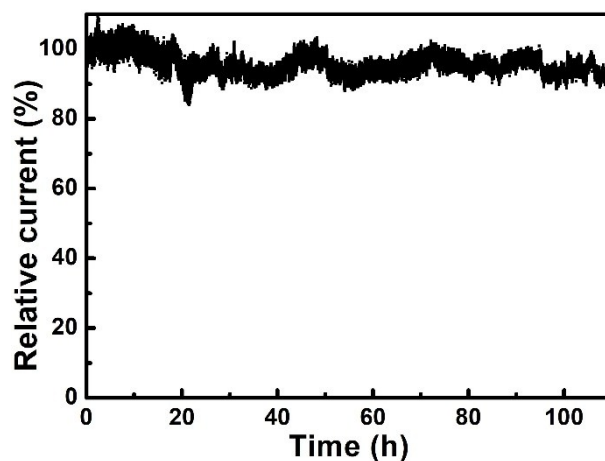


Fig. S13 Chronoamperometry test of the Ru/Y(OH)₃ NHs performed at the overpotential for 10 mA cm⁻².

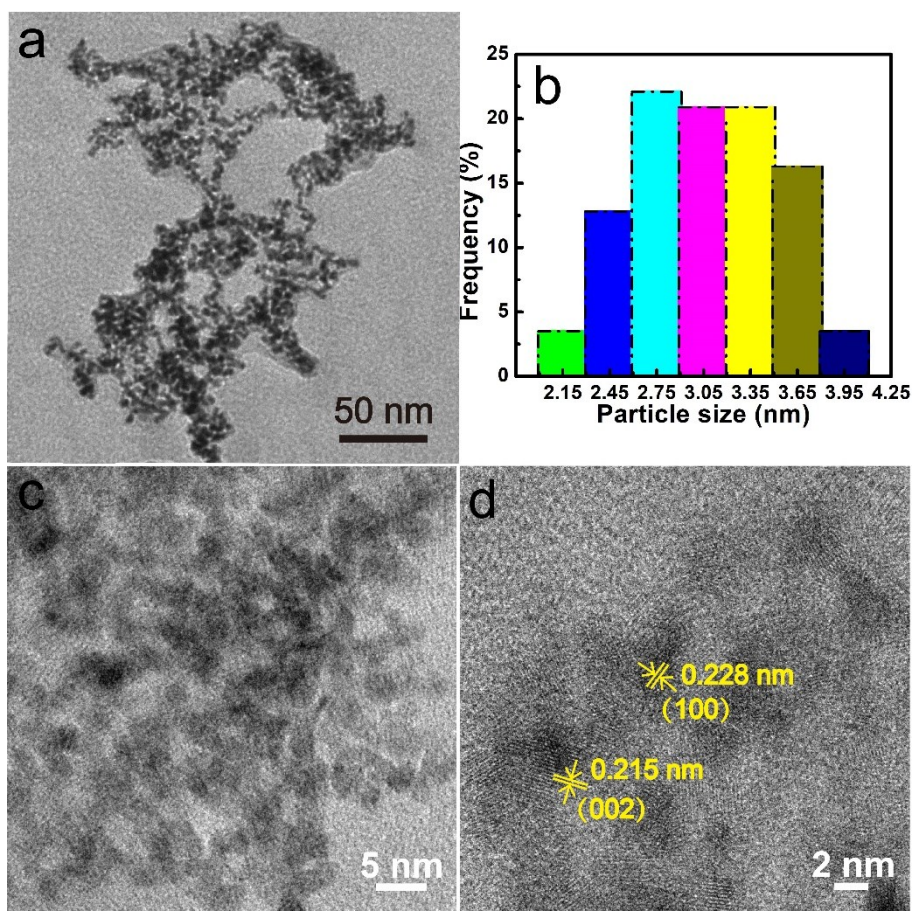


Fig. S14 (a) TEM, (b) size distribution, and (c, d) HRTEM images of the product after 20000 cycles durability test for Ru/Y(OH)₃.

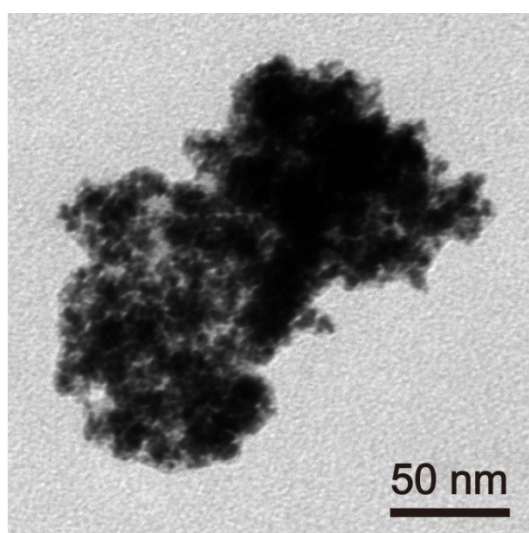


Fig. S15 TEM image of the product after 20000 cycles durability test for Ru NPs.

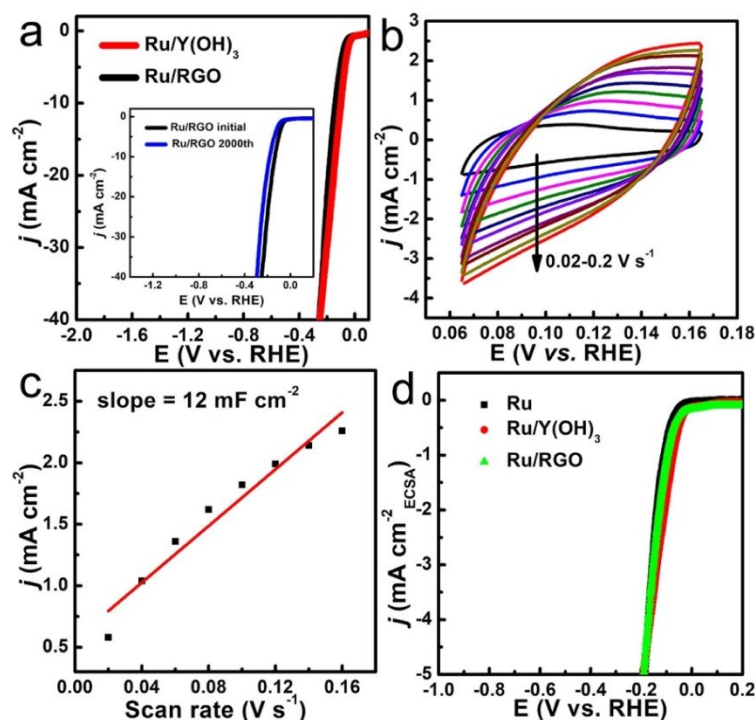


Fig. S16 (a) HER polarization curves for the Ru/Y(OH)₃ NHs and Ru/RGO catalysts. (b) Cyclic voltammogram curves and (c) calculated electrochemical double-layer capacitances (C_{dl}) for the Ru/RGO catalyst. (d) The polarization curves of Ru, Ru/RGO and Ru/Y(OH)₃ normalized to electrochemical surface area. The inset of **Fig. S16a** is the durability test of Ru/RGO for 2000 cycles.

In **Fig. S16a**, Ru/RGO catalyst displays similar polarization curve as Ru/Y(OH)₃ due to the superior conductivity of RGO, but the durability of Ru/RGO is worse than that of the Ru/Y(OH)₃, indicating the important role of Y(OH)₃. **Fig. S16d** shows the polarization curves of Ru, Ru/RGO and Ru/Y(OH)₃ normalized to electrochemical surface area (ECSA), and the ECSA value (cm_{ECSA}^2) is calculated from C_{dl} (mF cm^{-2}) and the specific capacitance value for a flat surface ($40 \mu\text{F cm}^{-2}$) using the following formula:

$$A (\text{cm}_{ECSA}^2) = C_{dl} (\text{mF cm}^{-2}) / 40 (\mu\text{F cm}^{-2})$$

From **Fig. S16d**, slightly better onset potential is observed for the Ru/Y(OH)₃, proving the improvement effect of Y(OH)₃ in facilitating water dissociation kinetics.

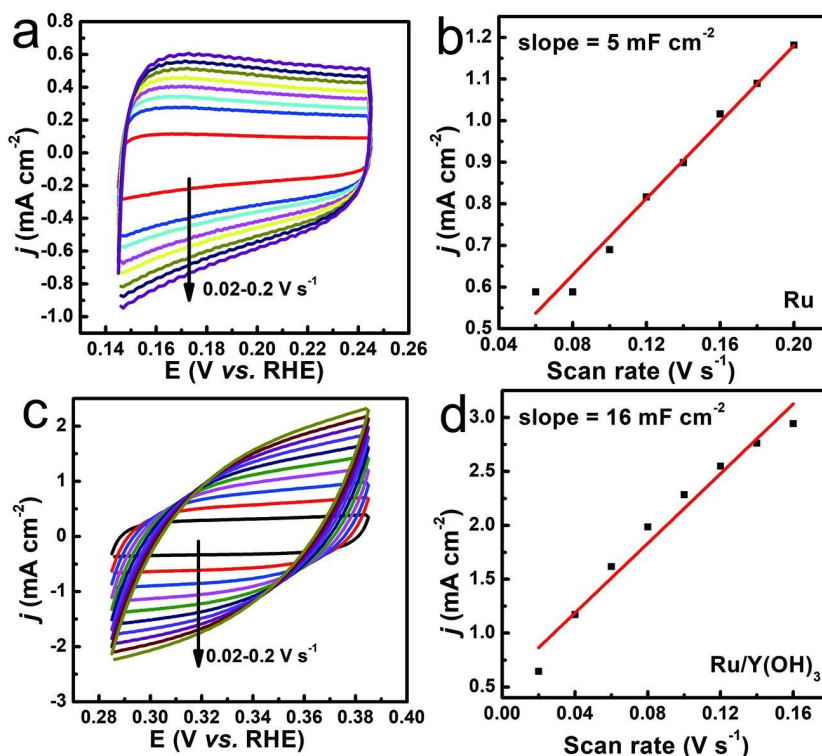


Fig. S17 Cyclic voltammogram curves for (a) Ru and (c) Ru/Y(OH)₃ at various scan rates (0.02-0.2 V s⁻¹). The calculated C_{dl} for the (b) Ru and (d) Ru/Y(OH)₃ catalysts. C_{dl} can be used to represent the ECSA of the catalysts, and a larger ECSA indicates more active sites are available to promote the hydrogen evolution reaction.

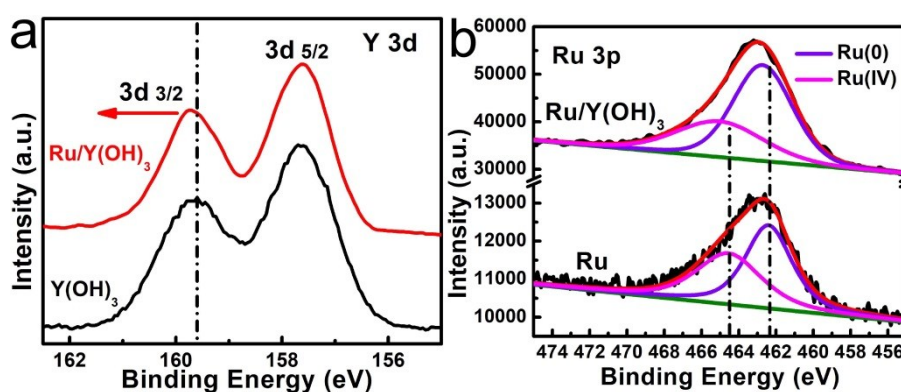


Fig. S18 Comparisons of the (a) Y 3d and (d) fitted Ru 3p core level XPS spectra for sole Ru and Ru/Y(OH)₃ NHs.

Fig. 4c, 4d and S18 show the XPS results for Y(OH)₃, Ru and Ru/Y(OH)₃ NHs. As displayed in **Fig. S18a**, two Y 3d signal peaks located at 157.6 eV (3d 5/2) and 159.6 eV (3d 3/2) were observed for sole Y(OH)₃, which are consistent with the reported

values for $\text{Y}(\text{OH})_3$.² Furthermore, the Y 3d binding energy for the Ru/ $\text{Y}(\text{OH})_3$ NHs slightly shifted in the high-energy direction compared to that of sole $\text{Y}(\text{OH})_3$, while the O 1s binding energy displayed a negative shift (**Fig. 4d**). In the Ru 3p core level spectra, the binding energy of the Ru/ $\text{Y}(\text{OH})_3$ NHs shifted in the high-energy direction compared to that of sole Ru (**Fig. 4c**). These shifts indicate partial electron transfers from both Y and Ru to O and electronic interactions between Ru and the hydroxyl groups in the $\text{Y}(\text{OH})_3$ scaffold. **Fig. S18b** shows the deconvoluted Ru 3p spectra for sole Ru and Ru/ $\text{Y}(\text{OH})_3$ NHs. The predominant peak located at 462.1 eV is assigned to Ru(0), and the other peaks are affiliated with ruthenium oxide.³ The small amounts of ruthenium oxide are attributed to surface oxidation of the Ru NPs.

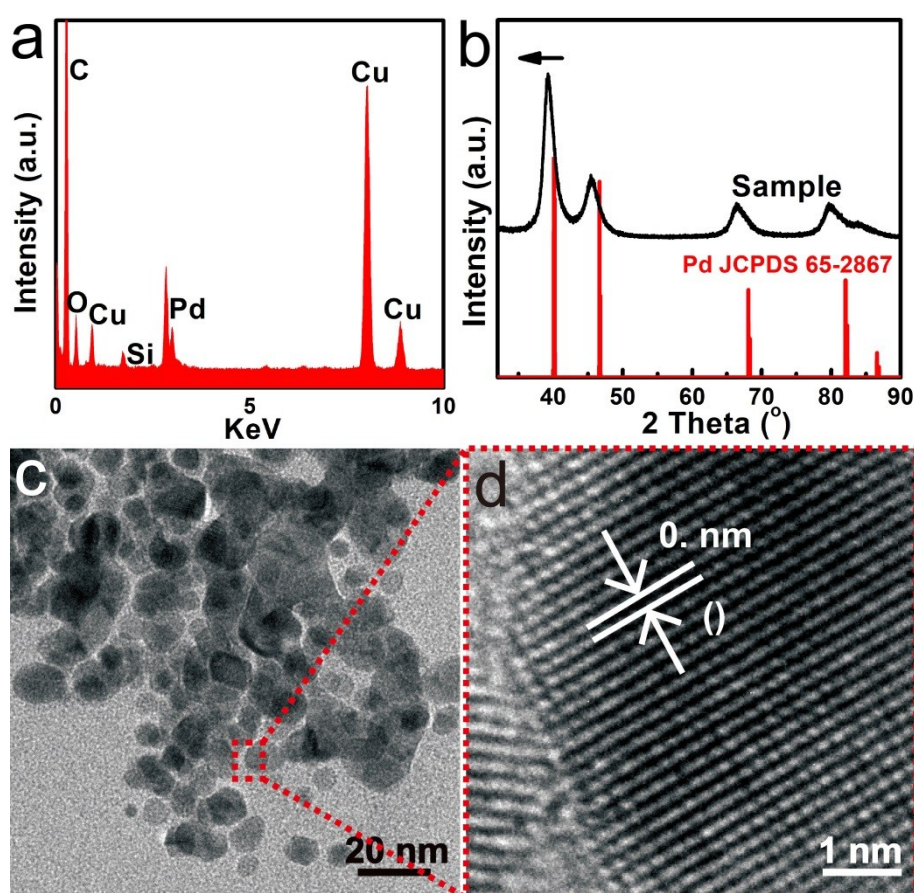


Fig. S19 (a) EDS, (b) XRD pattern, (c) TEM and (d) HRTEM images of Pd NPs.

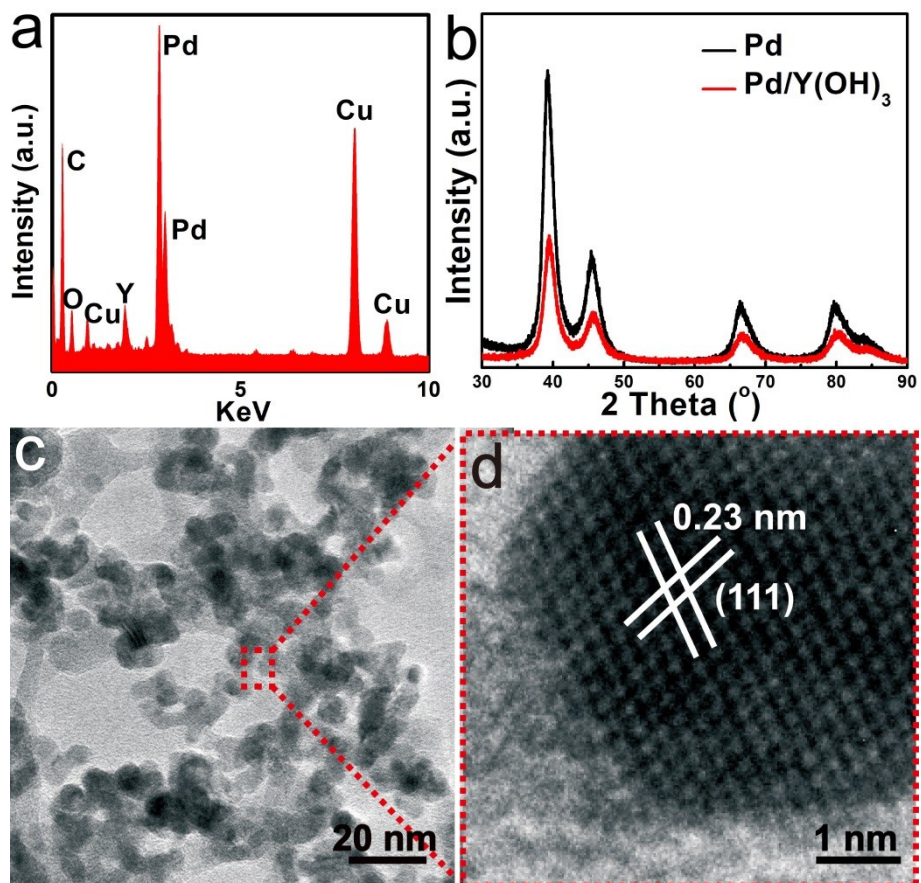


Fig. S20 (a) EDS, (b) XRD pattern, (c) TEM and (d) HRTEM images of Pd/Y(OH)₃ product.

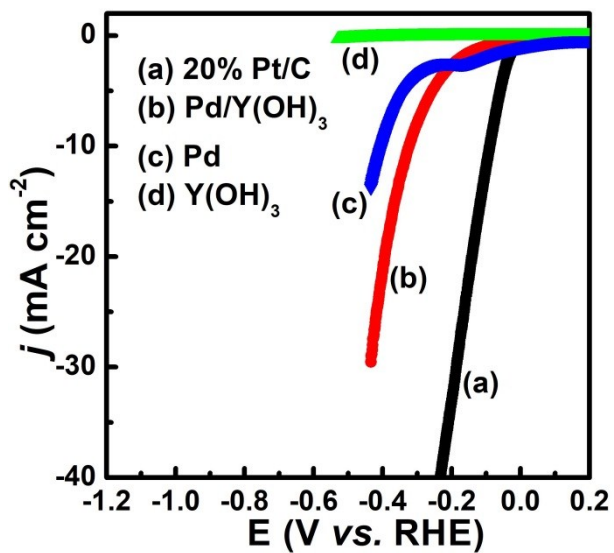


Fig. S21 HER polarization curves for the Pd, Y(OH)₃, Pd/Y(OH)₃ NHs and 20% Pt/C catalysts.

References

1. (a) Y. Zhang, B. Ouyang, J. Xu, S. Chen, R. S. Rawat and H. J. Fan, *Adv. Energy Mater.*, 2016, **6**, 1600221; (b) T. S. Kim, H. J. Song, J. C. Kim, B. Ju and D. W. Kim, *Small*, 2018, **14**, 1801284; (c) S. Huang, Y. Meng, S. He, A. Goswami, Q. Wu, J. Li, S. Tong, T. Asefa and M. Wu, *Adv. Funct. Mater.*, 2017, **27**, 1606585; (d) Z. Peng, S. Yang, D. Jia, P. Da, P. He, A. M. Al-Enizi, G. Ding, X. Xie and G. Zheng, *J. Mater. Chem. A*, 2016, **4**, 12878; (e) X. Fan, H. Zhou and X. Guo, *ACS Nano*, 2015, **9**, 5125; (f) M. Li, T. Liu, X. Bo, M. Zhou and L. Guo, *J. Mater. Chem. A*, 2017, **5**, 5413; (g) H. B. Wu, B. Y. Xia, L. Yu, X. Y. Yu, X. W. Lou, *Nat. Commun.*, 2015, **6**, 6512; (h) H. Du, R. Kong, F. Qu and L. Lu, *Chem. Commun.*, 2018, DOI: 10.1039/c8cc06331a; (i) K. Xu, H. Ding, M. Zhang, M. Chen, Z. Hao, L. Zhang, C. Wu and Y. Xie, *Adv. Mater.*, 2017, **29**, 1606980; (j) C. Y. Son, I. H. Kwak, Y. R. Lim and J. Park, *Chem. Commun.*, 2016, **52**, 2819; (k) Z. H. Xue, H. Su, Q. Y. Yu, B. Zhang, H. H. Wang, X. H. Li and J. S. Chen, *Adv. Energy Mater.*, 2017, **7**, 1602355; (l) J. Tian, Q. Liu, A. M. Asiri and X. Sun, *J. Am. Chem. Soc.*, 2014, **136**, 7587; (m) Y. Liang, Q. Liu, A. M. Asiri, X. Sun, Y. Luo, *ACS Catal.*, 2014, **4**, 4065; (n) Y. Jia, L. Zhang, G. Gao, H. Chen, B. Wang, J. Zhou, M. T. Soo, M. Hong, X. Yan, G. Qian, J. Zou, A. Du, X. Yao, *Adv. Mater.*, 2017, **29**, 1700017; (o) Z. Huang, C. Lv, Z. Chen, Z. Chen, F. Tian and C. Zhang, *Nano Energy*, 2015, **12**, 666.
2. D. Majumdar and D. Chatterjee, *J. Appl. Phys.*, 1991, **70**, 988.
3. Z. Zhang, Y. Liu, B. Chen, Y. Gong, L. Gu, Z. Fan, N. Yang, Z. Lai, Y. Chen, J. Wang, Y. Huang, M. Sindoro, W. Niu, B. Li, Y. Zong, Y. Yang, X. Huang, F. Huo, W. Huang and H. Zhang, *Adv. Mater.*, 2016, **28**, 10282.